

# THE COMPLEMENTARY ROLES OF FEEDBACK AND MERGERS IN BUILDING THE X-RAY CORONAE OF MILKY WAY-SIZED HALOS

A. SOKOŁOWSKA<sup>1</sup>, A. BABUL<sup>1,2</sup>, L. MAYER<sup>1</sup>, S. SHEN<sup>3</sup>, & P. MADAU<sup>1,4</sup>

<sup>1</sup>Center for Theoretical Astrophysics and Cosmology, University of Zurich, Winterthurerstrasse 190, Zurich, Switzerland.

<sup>2</sup>Department of Physics and Astronomy, University of Victoria, Elliot Bldg, 3800 Finnerty Rd, Victoria, Canada.

<sup>3</sup>Institute of Theoretical Astrophysics, University of Oslo, Sem Saelands vei 13, Svein Rosselands hus, 0371 Oslo, Norway.

<sup>4</sup>Department of Astronomy and Astrophysics, 1156 High Street, University of California, Santa Cruz CA 95064, USA.

## ABSTRACT

We use cosmological hydrodynamical simulations of Milky Way-sized halos with different feedback strengths or merger histories to investigate the formation of X-ray luminous coronae. We show that a galactic corona is not a consequence of hot spherical accretion onto a galaxy but of mergers-induced shock heating and supernova feedback. Coronae grow inside-out and detach galaxies from the filamentary network as they outbalance the pressure of cold flows. Additionally, ram pressure strips cold flows at the intersection of the two fronts. Coronae thus drive the transition from the cold mode to hot mode accretion. Our results predict the presence of gas at high temperatures even as early as  $z = 3 - 4$ , and in halos of much lower mass than the critical mass for hot mode accretion suggested by previous simulations and analytical models (Dekel et al.). All this is quite different from the standard picture in which diffuse halos are a consequence of the thermalisation of kinetic energy derived from gravity and/or the geometric effect of cross sections of halos vs. filaments, and may be more relevant for halos harbouring typical spiral galaxies. We show that SN feedback impacts the galaxy-cold flows connection, which has also consequences for the large-scale gas supply and may contribute to galaxy quenching.

## 1. INTRODUCTION

Normal galaxies observed today are surrounded by envelopes of diffuse gas, which can attain temperatures exceeding  $10^5 - 10^6$  K (see the review on gaseous halos by Putman et al. 2012). Such media have already been detected in ultraviolet and X-ray absorption lines (Sembach 2006; Wang et al. 2005; Bregman & Lloyd-Davies 2007; Peebles et al. 2014; Miller & Bregman 2014; Fang et al. 2015), in OVIII emission (Gupta et al. 2009; Henley & Shelton 2013), and as excess X-ray emission relative to the background (Rasmussen et al. 2009; Anderson & Bregman 2011; Bogdán et al. 2013; Tumlinson et al. 2011). The direct detection of hot halo gas ( $T > 10^6$  K) at extragalactic distances is currently possible only around massive galaxies (e.g. Anderson & Bregman 2011; Bogdan et al. 2013), but in the future a more sensitive X-ray observatory such as *Athena+* may bring spatially resolved images also of lower-mass spirals (Kaastra et al. 2013). For the time being, the hot halo around our Galaxy is the best probe of hot halos around lower-mass galaxies ( $M_{halo} \simeq 10^{12} M_{\odot}$ ).

Recent modelling of a million degree gaseous halo in the Milky Way results in a hot halo mass estimate of  $M(200kpc) = 3.8 \times 10^{10} M_{\odot}$  (Miller & Bregman 2013).

The question of the origin of diffuse gas has been under investigation for several decades. Until about a decade ago, the standard paradigm of galaxy formation assumed that dark matter relaxes to a virial equilibrium, and gas follows the dark matter during collapse (Rees & Ostriker 1977; White & Rees 1978). The resulting supersonic accretion triggers an accretion shock (Binney 1977). The shock develops at the virial radius or closer to the galaxy, depending on the ratio of the cooling and dynamical timescales (White & Frenk 1991). In this framework, halos in the mass range  $M_{halo} \simeq 10^{12-13} M_{\odot}$  are expected to support an accretion shock at their virial radius, and thus contain a quasi-hydrostatic atmosphere of hot gas. A detailed analytical treatment of shock stability in Birnboim & Dekel (2003) brought down the critical halo mass for a stable shock at the virial radius to over  $10^{11} M_{\odot}$  for primordial gas and around  $10^{12} M_{\odot}$  for solar metallicity gas. The accretion shock relies on the presence of a stable atmosphere of post-shock gas to support itself.

However, both the models of White & Frenk (1991);

Birnboim & Dekel (2003) assumed spherical symmetry, and thus could not capture the scenario of asymmetric halo configurations. 3D simulations have revealed that most of the gravitational cooling radiation comes from gas at temperatures far below the typical virial temperatures of galaxies (Fardal et al. 2001), and that a significant fraction of gas in galaxies at the low-mass end of this range has never been shock heated (Katz et al. 2003; Kereš et al. 2005, 2009; Dekel et al. 2009; Brooks et al. 2009). Kereš et al. (2005, 2009) showed that, for all halos below a critical mass of  $3 \times 10^{11} M_{\odot}$  and at redshifts in range  $z = 0 - 3$ , the infall is predominantly cold. In fact, these simulations have identified two thermodynamically and geometrically distinct modes of accretion: “cold mode” (filamentary inflow resulting in the maximum gas temperature that is lower than the virial temperature) and “hot mode” (spherical accretion with heating of gas up to  $T > 10^{5-7}$  K before cooling, see also Dekel & Birnboim 2006; Kereš et al. 2009; Dekel et al. 2009). The diffuse X-ray luminous halo is thus generated by the hot mode accretion, in halos which grow sufficiently in mass (i.e. beyond the critical mass threshold). The time of this transition depends on the halo growth rate but is often seen around  $z \sim 2$ . This picture, however, has yet to be reassessed in the presence of effective feedback scheme preventing excessive star formation, particularly in the high redshift universe, which was foreshadowed by White & Frenk (1991). This is the main topic of this paper.

We focus on the Milky Way mass scale in order to probe the impact of supernova feedback on the evolution of the diffuse halo. This is motivated by the observed presence of both gas at  $T \simeq 10^{5-6}$  K and significant mass of cold, neutral gas in high velocity clouds (Putman et al. 2003). The simultaneous existence of both phases of gas suggests that the Milky Way ( $M_{halo} \simeq 10^{12} M_{\odot}$ ) is undergoing a transition between cold and hot accretion. Supernova feedback is still very important on this mass scale (see a review of Somerville & Davé 2015). It is a crucial ingredient for regulating star formation in galaxies and drive winds. Either alone or in combination with other stellar feedback processes, such as radiation pressure or photoionization, is crucial to obtain realistic stellar and baryonic masses and star formation efficiencies, perhaps up to a mass scale as large as  $10^{13} M_{\odot}$ , and especially as it shapes the lower-mass end of the galaxy mass function (e.g. Bower et al. 2012; Puchwein & Springel 2013). Various forms of stellar and SN feedback can reproduce the structure of disk galaxies satisfactorily, both at the level of global parameters and internal properties in various mass ranges (dwarfs: Shen et al. (2014); spiral galaxies: Guedes et al. (2011), Marinacci et al. (2014), Agertz & Kravtsov (2015), Roškar et al. (2014); massive early-

types: Fiacconi et al. (2014)).

van de Voort et al. (2016) have shown that the diffuse X-ray luminosity around galaxies correlates with the star formation rate up to a few times  $10^{12} M_{\odot}$ , as expected if feedback plays a role in the origin of an extended gaseous corona up to a certain mass scale. However, a detailed study of its impact on the build-up on the hot mode in high-resolution simulations is lacking. We thus test the possibility that hot diffuse galactic coronae do not reflect shock-heating induced by gravitational infall, rather are the consequence of feedback-driven heating and outflows. This is particularly important from the point of view of galaxy formation, as the transition from cold to hot accretion seems to be the key to galaxy quenching (Dekel & Birnboim 2006). Observations reveal a robust bimodality in the galaxy population which divides into the so-called blue and red sequences. The threshold for the transition between these sequences is  $3 \times 10^{10} M_{\odot}$  (equivalent to a critical halo mass of  $\simeq 10^{12} M_{\odot}$ ).

In the previous paper (Sokolowska et al. 2016, hereafter Paper I), we studied present-day diffuse halos of Milky Way-sized galaxies using a suite of zoomed-in simulations. Our foundational model, Eris, employs subgrid physical recipe for supernova feedback, which turned out to be successful in reproducing a realistic Milky Way-like galaxy (Guedes et al. 2011). We showed in Paper I that this recipe also results in a realistic present-day gaseous halo with key properties being in agreement with recent constraints: namely, a X-ray luminosity in the 0.5-2 keV band of  $\sim 10^{39}$  erg/s; coronal density sufficient to ram-pressure strip Milky Way satellites; and radial halo electron density profile consistent with that implied by the OVII absorption line measurements (see Paper I for the details). Additionally, we studied a run with much stronger supernova feedback in the same context, E2k (Shen et al. 2012). We identified a feature in our simulated galaxies that we referred to as *a corona*. Coronae are central regions of hot gas with temperatures exceeding  $10^6$  K, characterised by approximately spherical geometry and a high degree of localization, as they tend to extend no farther than 100-140 kpc ( $0.6 r_{vir}$ ). They are embedded in massive reservoirs of baryons of  $T = 10^{5-6}$  K.

In this second paper in the series, we address the question of their origin. We investigate the key physical processes that build the MW-like halos and their coronae, including supernovae (SN) feedback and merger-induced shocks, both of which are known to raise the temperature of the halo gas. To do so, we run a default subgrid model of Eris with SN feedback off, ErisNFB, and compare the resultant halo with the original variant of Eris. This work also includes a new run in the inventory of our hydrodynamical zoom-in simulations,

namely Venus, which represents a case with a violent merger history (Sokolowska et al. 2017).

This paper is outlined as follows. In section 2 we motivate why we investigate this particular set of runs and describe the physics included in the simulations. Section 3 contains our results in the context of the inside-out growth of the coronae and the role of feedback in their formation. We also explore the connection between the growth of coronae and the cold filamentary network. This is then followed by the summary in section 4.

## 2. SIMULATIONS

We use two unique high-resolution simulations of spiral galaxies, Eris and Venus, performed with the tree-smoothed particle hydrodynamics (SPH) code GASOLINE (Wadsley et al. 2004) with mass resolution  $m_{\text{dm}} \simeq 9.8 \times 10^4 M_{\odot}$  and  $m_{\text{SPH}} \simeq 2 \times 10^4 M_{\odot}$ , and spatial resolution  $\simeq 120$  pc. These runs are all cosmological zoom-in simulations of Milky Way-sized galaxies. Additionally, we investigate the consequences of the exclusion of feedback (model of Eris without supernova feedback, see section 3.2), as well as include a discussion of the impact of enhanced feedback on our results (model E2k, see the Appendix).

The first of the runs, Eris, has been shown to be successful in matching various properties of late-type spirals such as the Milky Way (Guedes et al. 2011). The second run, Venus, adopts the same subgrid model as Eris but with different initial conditions (IC). These ICs were chosen to have an active merging history down to a low redshift in contrast to the quiet merging history of Eris, while at the same time ensuring that final virial halo mass ( $\sim 8 \times 10^{11} M_{\odot}$ ) and a halo spin parameter ( $\lambda \sim 0.03$ ) are the same in both Eris and Venus.

Both simulations include radiative and Compton cooling. The radiative cooling is computed for a simple mixture of H and He via non-equilibrium cooling rates in the presence of the ionizing cosmic ultraviolet (UV; Haardt & Madau 1996) background (Wadsley et al. 2004). Additionally, gas of  $T < 10^4$  K can cool through fine structure and metastable lines of C, N, O, Fe, S, and Si (Bromm et al. 2001; Mashchenko et al. 2007).

The recipes for star formation and SN feedback are the same in all the runs and are described in Stinson et al. (2006). Briefly, gas particles must be dense – namely have a density above the threshold  $n_{\text{SF}}$  (5 atom  $\text{cm}^{-3}$ ) – and cool (cooler than  $T_{\text{max}} = 10^4$  K) in order to form stars. Particles that fulfill these requirements are stochastically selected to form stars according to  $dM_*/dt = c^* M_{\text{gas}}/t_{\text{dyn}}$ , where  $M_*$  is the mass of stars created,  $c^*$  is a constant star formation efficiency factor (set to 0.1 in all runs),  $M_{\text{gas}}$  is the mass of gas creating the star, and  $t_{\text{dyn}}$  is the gas dynamical time. Each star particle then represents a population of stars, cov-

ering the entire initial mass function (IMF). We adopt the Kroupa et al. (1993) IMF.

In all the runs, metals come from SNI and SNI (Stinson et al. 2006). Stars more massive than  $8 M_{\odot}$  explode as SNI. According to the “blastwave feedback” model of Stinson et al. (2006), feedback is purely thermal, as the blastwave shocks are expected to convert the kinetic energy of ejecta into thermal energy on scales smaller than those resolved by our simulations. Once energy is ejected (the fraction of SN energy that couples to the interstellar medium is  $\epsilon_{\text{SN}} = 0.8$ ), particles receiving the energy are prevented from cooling for typically 10–50 Myr, with the cooling shut-off timescale being computed as the sum of the Sedov–Taylor (Taylor 1950; Sedov 1959) and snow-plough phases in the ejecta (McKee & Ostriker 1977). By delaying the cooling, we model in a phenomenological way the unresolved effect of momentum and heating by turbulent dissipation in the ejecta before they reach the radiative phase. Delaying the cooling also prevents artificial overcooling of gas heated by SN feedback. The strength of feedback depends on the number of SNe produced, which is in turn governed by the IMF and, locally, by the star formation density threshold.

The Venus simulation employs different initial conditions than Eris. The ICs of Eris were generated with GRAFIC2 (Bertschinger 2001). The “zoom-in” of Venus was initialized using the MUSIC code (Hahn & Abel 2011), which allows a computationally more efficient topological identification of the Lagrangian subvolume for the refinement. Eris and Venus both form at the intersection of four dark matter filaments, but their convergence pattern is different (see Figure 1). In general, Venus experiences twice as many major mergers as Eris, with the last major merger (defined as a merger with mass ratio  $> 0.1$  between the two galaxies) occurring at  $z = 0.9$ , as opposed to  $z = 3.1$ . While in Eris, a central dominant halo assembles very early, in Venus, multiple progenitors of comparable mass evolve separately for a long time, with one single halo and its associated galaxy only appearing after the last major merger at  $z < 0.9$ . The amount of substructure at  $z = 0$  is also more abundant in Venus relative to Eris, both in the stellar and in the dark matter component. In particular, a large satellite orbits around the primary galaxy in Venus even at late times, causing a perturbation on the main disk at pericenter passages, the last of which induces perturbations in the structure of the main disk as late as  $z = 0.24$ .

## 3. RESULTS

In Paper I, we defined the hot corona to be the gas at  $T > 10^6$  K localized in a spherical region around the main galaxy with a radius of about 100 kpc at  $z = 0.5$  (140 kpc at  $z = 0$ , equivalent to  $0.6 R_{\text{vir}}$ ). We observed

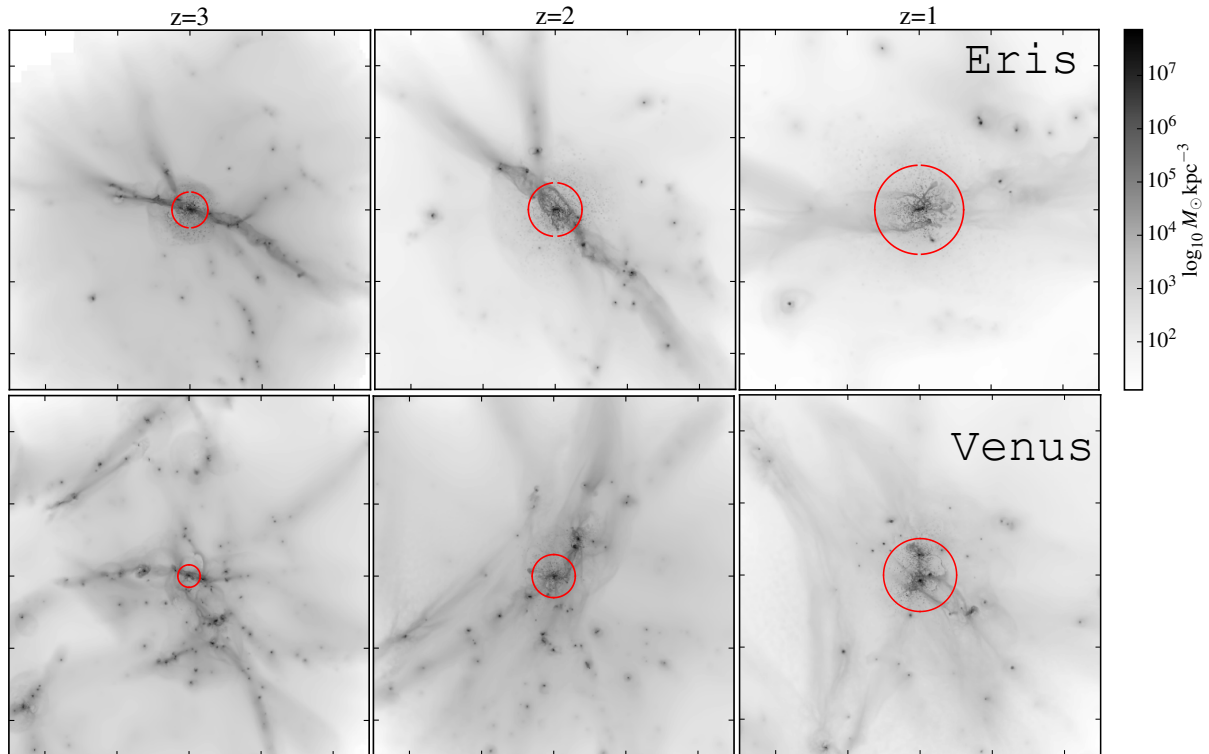


**Figure 1.** Density maps of gas around edge-on galaxies in two examples of initial conditions: quiet (Eris) and active (Venus). Width of each square is 1 comoving Mpc. The cross sections of the halo at each time step are shown as red circles.

that gaseous halo undergoes a transformation over time that creates an onion-like structure, with the hot corona being embedded in the warm-hot ( $10^5\text{--}6$  K) envelope rich in baryons. The properties of this diffuse gas in Eris turned out to be in good agreement with a range of observational constraints on the Milky Way halo gas, including the X-ray luminosity in the 0.5-2 keV band (Snowden et al. 1997; Wang 1998; Miller & Bregman 2014,  $\sim 10^{39}$  erg/s).

Here, we start by assessing Venus. As previously, we compute the X-ray luminosity of all its gas particles that can be found within the virial radius of a halo. Our calculation is based on the radiative rates of Astrophysical Plasma Emission Code3 (APEC) (Smith et al. 2001), which assumes the optically thin gas in collisional ionization equilibrium (for more details on the calculation, see Paper I). With this method, the X-ray luminosity of Venus is  $L_X = 1.2 \times 10^{39}$  erg/s, hence also in good agreement with the Milky Way observations.

Figure 2 compares temperature maps of gas of Eris

and Venus at three different time steps:  $z = 4, 3, 0.5$ . The configuration of the filamentary network of these two simulations is different, resulting in two distinct evolutionary sequences for the gas. For example, at  $z = 4$ , cold flows penetrate the halos of both of the main progenitors but gas in Eris is hotter. At  $z = 3$ , a hot bubble of gas in Eris is associated with single main progenitor, whereas in Venus diffuse gas is distributed among multiple progenitors. By  $z = 0.5$  Venus acquires a similar corona as Eris, albeit through a different evolutionary pathway.

The existence of similar diffuse halos that appear in different environments opens a question of what governs their evolution, and how they arrive at this end-state. In what follows, we investigate which processes are essential for explaining their origin. Then, we focus our attention on the role of supernova (SN) feedback in shaping these halos. Finally, we discuss the impact of growing hot coronae on the transition from cold filamentary to hot quasi-spherical accretion mode.

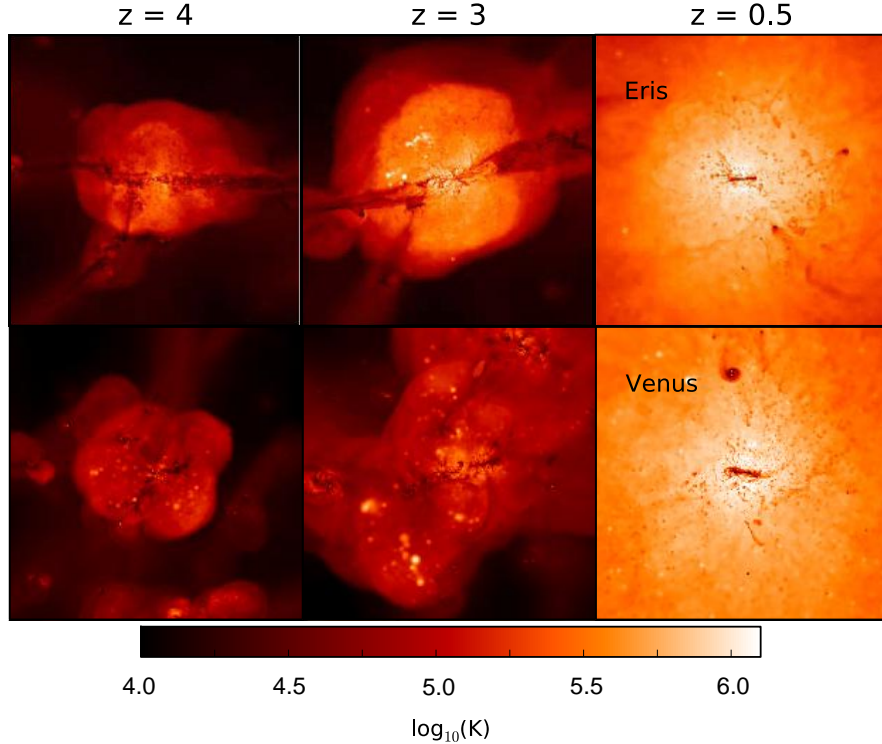


**Figure 2.** Two pathways to the same result: a galaxy surrounded by an X-ray-bright corona. Temperature maps of the gaseous halo of Venus and Eris are shown at three various timesteps. The width of each square is 300 comoving kpc. Compare with Fig. 1 of Sokolowska et al. (2016).

### 3.1. Growth of the diffuse medium

The conventional description of the formation of diffuse X-ray luminous halos assumes that they are generated due to the hot mode accretion, in halos which grow sufficiently in mass (i.e. beyond the critical mass threshold). Here, we test the validity of this scenario in our simulations. First, we investigate when halos of our galaxies enter the critical mass regime; then, we compare the resulting redshift with the time, during which hot diffuse atmospheres of gas begin to appear around those halos.

In the left panel (a) of Figure 3, we show the total halo mass of Eris and Venus as a function of redshift. The grey band indicates the metallicity-dependent lower limit for the mass of the halo, necessary to develop a stable inner shock at  $0.1 R_{\text{vir}}$  and it covers a metallicity range of  $0.03Z_{\odot}$  to  $0.3Z_{\odot}$  (Dekel & Birnboim 2006). The critical mass for the development of the stable virial shock (at  $R_{\text{vir}}$ ) exceeds  $10^{12}M_{\odot}$  already at  $Z = 0.03Z_{\odot}$ , hence would fall in this diagram above the grey band. The blue band corresponds to the mass range of  $2 - 3 \times 10^{11} M_{\odot}$ , which was found to be the nearly constant critical mass threshold between  $z = 3$  and  $z = 0$  in the simulations of Kereš et al. (2009). Beyond that transition mass, simulated galaxies were able

to sustain atmospheres of hot virialized gas. In the right panel (b) of Figure 3, we show the gas mass budget of Eris and Venus at 6 different redshifts that is normalized to the virial mass of the halo at a corresponding redshift. Each gas mass budget is divided into gas phases: cold ( $T < 3 \times 10^4 \text{ K}$ ), warm ( $3 \times 10^4 \text{ K} < T < 10^5 \text{ K}$ ), warm-hot gas ( $T = 10^5 - 6 \text{ K}$ ) and hot ( $T > 10^6 \text{ K}$ ). This plot excludes gas in the galactic disk, i.e. all gas particles with densities higher than the star formation density threshold (5 atoms/cc), in order to isolate the gaseous halo. Note that any differences in the gas fraction between the runs can be attributed to their assembly history (e.g. relatively low gas fraction before  $z = 2$  in Venus is correlated with the later halo assembly). When the halo masses of Eris and Venus converge, and Venus settles down after the last major merger, final gas fractions of both runs ( $z = 0$ ) become very similar.

Our galaxies enter the regimes for hot mode accretion at different times: Eris crosses the blue band at  $z = 3$  and can develop a stable shock at  $0.1 R_{\text{vir}}$  after  $z = 2$ , but never the virial shock. Venus, on the other hand, attains a halo mass that exceeds both thresholds drawn with blue and grey bands later, i.e. between  $z = 2$  and  $z = 1.5$ . This implies that a significant fraction of diffuse gas (red and cyan bars in the panel (b) of Figure 3) should appear close to these redshifts. However, this

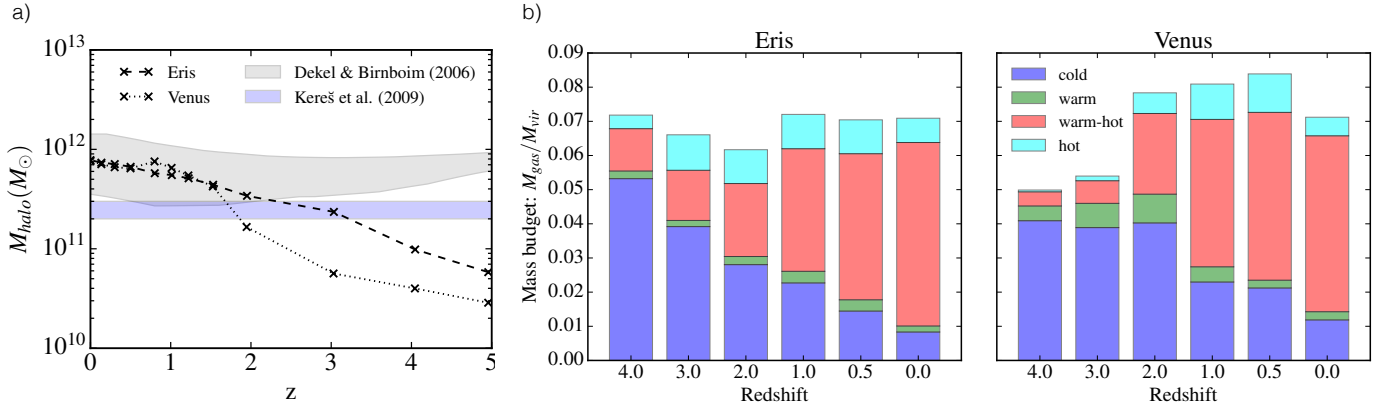


**Figure 3.** The stable shock condition vs. the formation of diffuse gas in halos. a) Halo mass as a function of redshift is compared with the critical mass for the development of a stable shock. The grey band represents the metallicity-dependent expectation for the critical mass necessary to develop a stable inner shock at  $0.1 R_{vir}$  (Dekel & Birnboim 2006, metallicity range 0-0.3  $Z_{\odot}$ ). The blue band marks a mass range of halos from Kereš et al. (2009) that can sustain atmospheres of hot, virialized gas. b) Gas mass budget of the gaseous galactic halos around galaxies at various redshifts, measured within their virial radii. Cold gas:  $T < 3 \times 10^4$  K; warm gas:  $3 \times 10^4 \text{K} < T < 10^5 \text{K}$ ; warm-hot gas:  $T = 10^{5-6} \text{K}$ ; hot gas:  $T > 10^6 \text{K}$ .

is not what we observe. Although the cold gas is the most abundant gas phase until  $z = 2$ , both halos can sustain hot and warm-hot atmospheres earlier than that. Taking the example of Eris, already at  $z = 4$ , the diffuse gas (warm-hot and hot combined) amounts to 40% of cold gas; at  $z = 3$ , to 70%. Diffuse gas appears in Venus way before the halo reaches the critical mass as well – at  $z = 4$ , it amounts to 12%, at  $z = 3$  to 25% and at  $z = 2$  to 75% of the cold gas, respectively. These results imply that hot accretion cannot be the source of diffuse halos developing at early redshifts.

Although hot gas is not the most abundant gas phase, it contributes the most to the X-ray emission and it can be observed in OVII/OVIII absorption/emission. Our diffuse halos match well these constraints, therefore we investigate under what conditions this agreement is achievable. We select particles, which are hot ( $T > 10^6$  K) at  $z = 0$  and at distances smaller than the virial radius, and trace their temperature and their time of accretion onto a halo. We treat a particle as accreted, if it crosses the virial radius of the halo for the first time. We show in Figure 4 that gas, which ends up in a hot corona at  $z = 0$  ( $T > 10^6$  K), does not come exclusively from late epochs. A significant fraction of gas building the present-day coronae is coming in at early times, and is cold as it passes the virial radius the first time. The contribution to the coronae of cold-accreted gas becomes negligible after 5-6 Gyrs of evolution (after  $z \sim 1.5$ ) in favor of the first-time warm-hot accretion. This significant mass of cold-accreted gas must then be heated to over a million degrees in order to become a part of a hot corona. In principle, stable inner shock

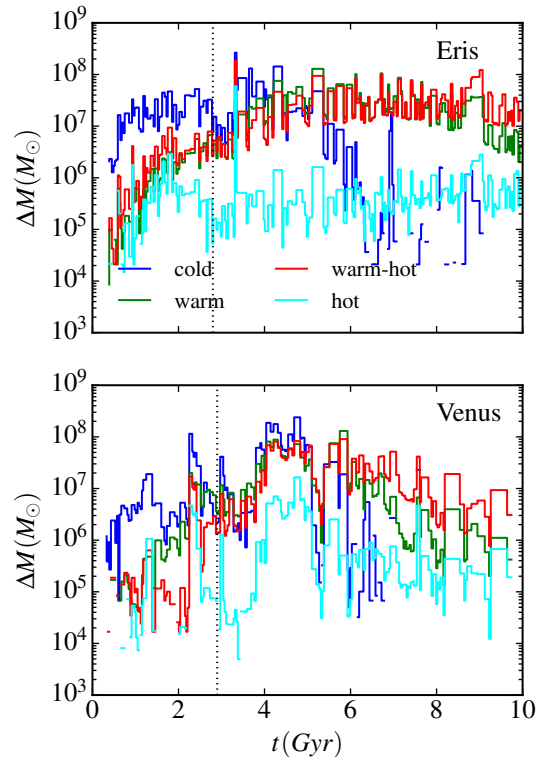


**Figure 4.** Temperature of gas particles present in a  $z = 0$  hot corona at first  $R_{vir}$  crossing, showing two-stage halo gas evolution. The dotted line marks approximately the time of the equivalence of the cold and hot mode accretion ( $z = 2.5$ ).

could be responsible for shock-heating of the cold infalling gas close to the center of the halo. However, we already showed this is impossible before  $z \sim 2$  (earlier

on,  $M_{\text{halo}}$  is below the grey band in Figure 3). Hence, cold-accreted gas must be either shock-heated via mergers and end up in a hot state with a very long cooling time, or it must be kept hot by the energy of supernovae (or both). It could also become a part of outflows and return as second-generation hot accretion at later times. The exact cause of the generation of hot coronae is the main topic of the paper, and we focus on this problem in the next section.

We note that the epoch of equivalence of cold and warm-hot accretion in Figure 4, as well as the time of the extinction of the cold accretion, are similar in these simulations for two different reasons. 1) The epoch of equivalence (dotted line in Figure 4) occurs at approximately  $z = 2.5$  in both runs, even though Venus and Eris are different in their halo mass by a factor of a few at that redshift (see Figure 3a). However, before  $z = 2$ , Venus experiences gas-rich mergers, which raise the diffuse gas fraction to the similar level as in Eris by  $z = 2$  (panel b of Figure 3). It is likely that the shock-heating from frequent mergers and/or accompanying SN blasts raised the temperature of gas both inside and outside the halo. As a result, the warm-hot accretion becomes important before halos acquire the critical mass. 2) The second similarity – the drop-off in the mass of cold-accreted gas near  $z \sim 1$  – is less surprising because the gravitational heating is expected to take over as soon as the simulations align in the  $M_{\text{halo}}(z)$  space and cross the blue and grey bands (Figure 3a).

In the rest of this section, we study the distribution of diffuse gas and characterize its thermodynamical state as a function of time. As previously, in the following analysis we remove those gas particles, which belong to the disk, i.e. discount all gas particles with densities higher than the star formation density threshold (5 atoms/cc).

First, we present the temperature profile of the gaseous halo in Figure 5. The mass-weighted average temperature of gas is calculated in the radial shells around the galactic center and normalized to the virial temperature of the halo, with  $T_{\text{vir}} = (GM_{\text{vir}}\mu m_p)/(2R_{\text{vir}}k_B)$  and assuming  $\mu \simeq 0.6$ . Virial temperature  $T_{\text{vir}}$  of the halo is  $(5.3, 7.5, 7.1, 6.8, 6.1) \times 10^5$  K for Eris and  $(2.9, 2.8, 4.5, 7.4, 6.0) \times 10^5$  K for Venus at  $z = (4, 3, 2, 1, 0.5)$ , respectively. One can distinguish two regions in these profiles that show different behavior with redshift, indicated by the black vertical line ( $r/r_{\text{vir}} = 0.06$ ) which marks the approximate extent of the disk at  $z = 0$ . Left of that line, gas cools over time to a fraction of the virial temperature, and supplies fresh gas to the galactic disk. Right of that line, the temperature increases over time relatively to the virial temperature of the halo. The distribution beyond the area of the galactic disk becomes peaked after  $z = 2$ . The peak is

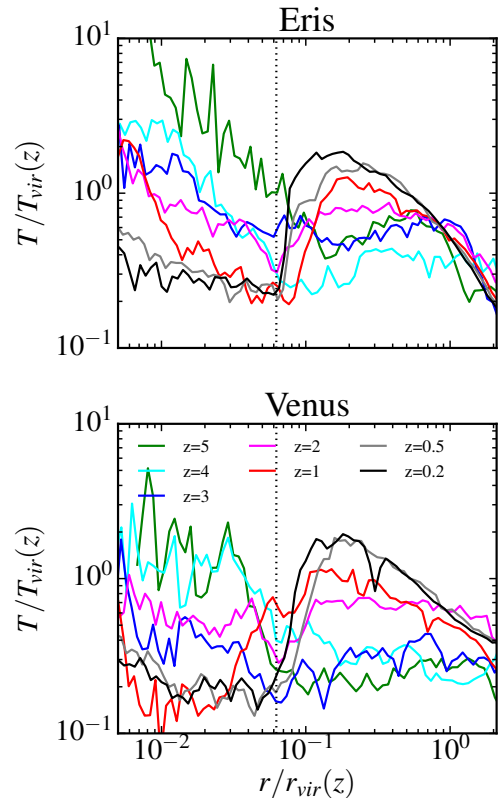


**Figure 5.** Radial distributions of gas temperature normalized to the virial temperature of the halo at a given redshift, showing the diffuse halo in formation. The vertical line marks the approximate extent of the disk at  $z = 0$ . Top to bottom: Eris, Venus.

localized near  $0.2R_{\text{vir}}$  (40 kpc at  $z = 0.2$ ), and attains its maximum at twice the virial temperature near the end of the calculation ( $z = 0.2$ ,  $\sim 2 \times 10^6$  K). Beyond  $R_{\text{vir}}$ , temperature fractions of  $T_{\text{vir}}$  are convergent, becoming nearly redshift-independent in Eris. The peak of the function  $T/T_{\text{vir}}$  in Figure 5 exposes that some heating process (or a combination of processes) is acting just above a disk, forming a hot corona.

Next, we divide the diffuse gas into hot ( $> 10^6$  K) and warm-hot ( $10^5$ – $10^6$  K) gas to study their spatial distribution. In Figure 6, we compare their density profiles at different redshifts. At first ( $z = 4$ ), warm-hot and hot gas in both simulations fall off monotonically with radius. After  $z = 2$ , however, striking differences arise: 1) the distribution of warm-hot gas has an inflection point around  $0.2 - 0.3R_{\text{vir}}$ , preceding a local maximum beyond this radius; 2) the drop-off of the density profile of hot gas becomes increasingly steeper. The steep drop-off indicates that hot gas can be found only within a fraction of a virial radius and not beyond. Thus, after  $z = 2$ , a hot corona of both galaxies becomes surrounded by warm-hot medium increasing in density, which is what

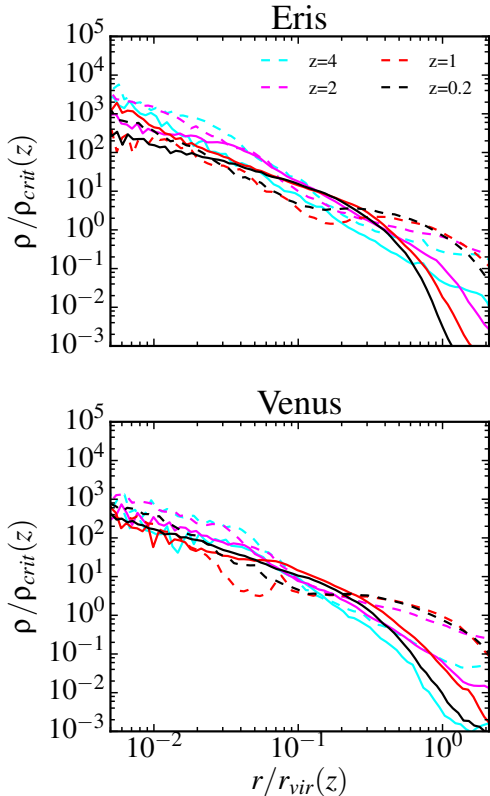


**Figure 6.** Radial density distribution of gas and its evolution with redshift. Dashed and solid lines denote the warm-hot and hot components of gas, respectively. Quantities are normalized to the critical density and the virial radius of the galaxy at a given redshift, and show the development of the onion-like structure: a corona embedded in the warm-hot soup of gas.

is seen in the end state. The envelope of warm-hot gas spreads out to a few virial radii.

We quantify the extent of hot gas as a function of time in Figure 7. As a proxy, we defined its extent as a radius encompassing 80% of its total mass within a virial radius ( $r_{80}$ ). We find that, before the formation time of the corona (around  $z = 4 - 3$ ), most of the hot gas spreads out to 80% of the virial radius. After  $z = 2$ , both hot halos are confined to  $0.4 R_{vir}$  at  $z = 0$ .

The grey-shaded region in Figure 7 shows, approximately within which radius cooling of hot gas proceeds on a timescale that is shorter than the Hubble time. To provide this estimate, we calculated cooling time as a function of radius based on the actual radiative cooling rates from the simulation,  $\Lambda$ , and the internal energy,  $U$ , according to  $t_{cool} = U/\Lambda$ . We verified that in both simulations the cooling time is very short near the galactic center (e.g., within  $0.1 r_{vir}$  it drops to orders of magnitude below 1 Gyr even at  $z = 1$ ), and monotonically increases with radius. At  $z = 3$ , hot gas within the virial radius cools on a less than 1 Gyr time scale. With the

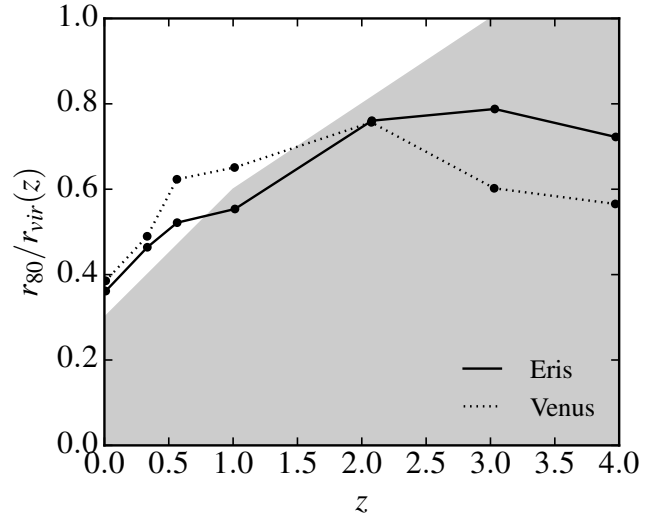


**Figure 7.** The size evolution of hot gas halo.  $r_{80}$ , defined as a radius encompassing 80% of its mass, is normalized to the virial radius ( $r_{vir}$ ). Grey-shaded region indicates where cooling of hot gas is still important (i.e.  $t_{cool} \ll t_{Hubble}$ ).

passage of time, cooling rate of the outer layer of the halo ( $r > 0.6 R_{vir}$  at  $z = 1$ ,  $r > 0.3 R_{vir}$  at  $z = 0$ ) increases to  $t_{cool} \gg t_{Hubble}$ . Thus, a hot corona heated inside-out would partially cool radiatively and partially adiabatically as it expands, transforming into the warm-hot phase of gas, and contributing to the local density peak of warm-hot gas past the inflection point in Figure 6. We refer to this transformation in the next section.

### 3.2. Role of feedback and mergers

In this section we investigate what the impact of major heating mechanisms is on the build-up of the diffuse halo. In particular, we determine whether the energy injection by feedback plays a role in building up a corona. The design of the code GASOLINE allows us to disentangle the following heating mechanisms per particle: heating due to atomic/radiative processes only ( $rad_{heat}$ ), supernovae thermal feedback ( $SN$ ), artificial viscosity ( $AV$ ), and work done by adiabatic contraction (or expansion, in which case  $pdV$  will be negative and hence contribute to adiabatic cooling). We are particularly interested in the relevance of each of these mechanisms for a build-up of two phases of gas: the warm-hot gas ( $T = 10^5 - 6 K$ ) and the hot gas ( $T > 10^6 K$ ). Hence, we measure the mass-weighted energy rates of those heating mechanisms within the virial radius per gas phase as a function of a redshift, and present them in Figure 8. We normalize all energy injection rates to the total heating rate  $\dot{E}_{sum} = \sum_i \dot{E}_i$ , where  $i$  stands for each of the processes mentioned above.

The lines in Figure 8 are color-coded according to the gas phase; the energy rates of warm-hot gas are denoted



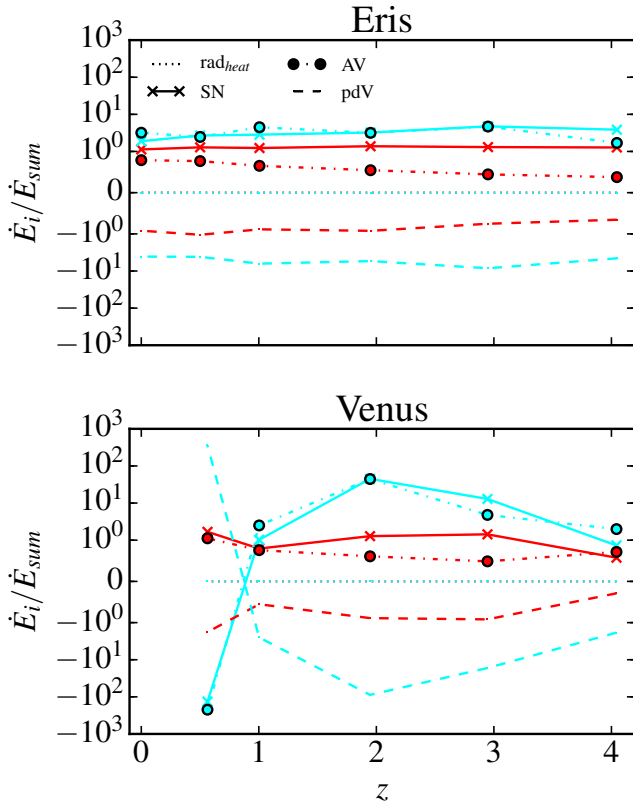


**Figure 8.** Energy injection rates for various gas phases in the region encompassed by a sphere of a virial radius around a galaxy, normalized to the total heating rate. The color coding corresponds to the warm-hot (red) and hot (cyan) gas phases. Legend:  $rad_{heat}$  – heating due to atomic/radiative processes only,  $SN$  – supernovae thermal feedback,  $AV$  – artificial viscosity,  $pdV$  – work done by/on the gas.

with red lines, and of hot gas with cyan lines. The  $pdV$  work of both phases is negative at all times, meaning that the diffuse gas is expanding, and thus adiabatically cooling. In fact, in the aftermath of a major merger at  $z = 0.9$ , hot gas of Venus cools adiabatically so efficiently that the net energy injection rate  $\dot{E}_{sum}$  becomes negative (hence  $\dot{E}_{SN}/\dot{E}_{sum} < 0$ ,  $\dot{E}_{pdV}/\dot{E}_{sum} > 0$ ).

The heating of the warm-hot gas is dominated by supernovae across all redshifts. The second-most important heating source of that phase is artificial viscosity, with a rate that is lower within a factor of two. The build-up of the hot phase, however, is approximately equally driven by both of these heating agents, as is shown with the cyan lines. We note that, as  $AV$  is only a tracer of shocks and not the measure of shock heating in these simulations, we treat it as such. The core result of this analysis is thus that, since supernovae heating is more, or at least equally, important source of heating, it must play a major role in shaping the diffuse halos of our galaxies.

Another argument pointing towards the relevance of feedback is the high metal enrichment of the diffuse gas both as early as  $z = 7$  and late as  $z = 0.5$ . Figure 9 shows radial distributions of metallicity of various phases of gas at 3 epochs:  $z = 7$ ,  $z = 3$ ,  $z = 0.5$ , assuming  $Z_{\odot} = 0.0194$  (Anders & Grevesse 1989). We use the results for Eris as an example of trends which are common for both simulations. As in the previous section, we are interested in the metallicity distributions in the gaseous halo only and not in the disk, therefore we discount particles above the star formation threshold. The resultant radial metallicity profiles of the halo gas show that the hot phase of gas is always the most metal-enriched. The warm-hot gas is second most metal-enriched to at least as far as 2 virial radii. Metals in our simulations come from SNI and SNIa.

The fact that  $SN$  feedback has a significant impact on the warm-hot gas phase explains the puzzling feature of the warm-hot density profile, which we discussed in the previous section (Figure 6). The warm-hot gas envelope forms at the intersection of outflowing material and warm-hot/hot intergalactic medium (IGM) accretion. This explanation is supported by the fact that hot gas is indeed adiabatically expanding. Moreover, metal-enriched outflowing warm-hot gas mixes with the hot/warm-hot IGM accretion, making it the second-most metal-enriched gas phase. This is illustrated in Figure 10, which summarizes the following experiment.

First, we divide a gaseous halo at  $z = 0$  into three distinct regions: 1) dominated by the disk ( $r_0 < 15$  kpc), 2) harboring a corona ( $r_0 \in (15, 100)$  kpc), 3) encompassing the extended warm-hot reservoir  $r_0 \in (100, 240)$  kpc. We measure the fractions of gas mass per gas phase in all these regions at  $z = 0$  (region 1: 90%, 1%, 4%, 5%; region 2: 9%, 0%, 58%, 33%; region 3: 2%, 3%, 92%, 3%; for cold, warm, warm-hot, hot phase, respectively). Then, we select randomly 100 particles according to these weights (e.g., the central region then consists of 90 cold, 1 warm, 4 warm-hot and 5 hot particles), and color-code them according to their final temperature at  $z = 0$ . Next, these representative particles are traced back in time to redshifts higher than  $z = 0$  and plotted on the radius-temperature ( $r - T$ ) diagrams (a corresponding movie can be found in the supplementary material). As a result, we are able to distinguish three different patterns of accretion, and capture their variations, which are dependent on the stage of the halo evolution. We show them in Figure 10, where we indicate the typical trajectories of particles with black arrows. The left and right columns of Figure 10 are examples of the first ( $z = 2.72$ ) and the second stages ( $z = 0.54$ ) of accretion. We use Eris as the case study.

The central region (top panel in each column) is always dominated by the “cold flows”. Even at a later

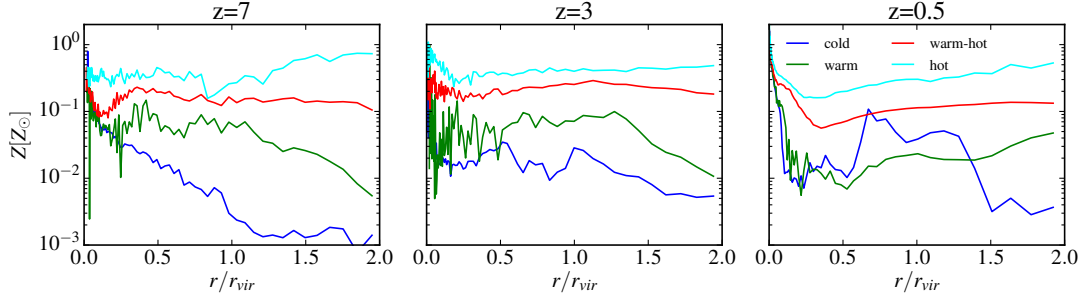


**Figure 9.** Example of radial metallicity profiles per gas phase at 3 different time steps. Case study: Eris. Profiles of Venus are very similar and show the same trend: hot gas is the most metal-enriched gas phase, and warm-hot gas is the second-most metal-enriched gas phase.

stage, when gas is heated up to  $10^5$  K upon entering the virial radius, its temperature drops down to below  $3 \times 10^4$  K while accreting. Although feedback dramatically increases the temperature of some gas particles, they manage to cool very rapidly and efficiently, hence on average they never migrate outwards.

The middle layer (second panel in each column) of a present-day gaseous halo is built by circulation flows. At first, gas enters the virial radius through cold flows, obtains SNe energy or shock-heats because of mergers, and is ejected outward, even beyond the virial radius. Then in the second stage, the trajectory of the incoming particles forks in the  $r - T$  diagram: some gas enters as relatively cool particles, and some is heated. At the end, the resultant high-temperature population ( $T > 10^5$  K) is formed at the intersection of freshly accreted gas (or re-accreted after the particles’ turnaround), and the gas in outflows.

Similarly to the middle layer, the outmost region (third panel) is first supplied by the warm/cold inflow of gas. However, outflows powered by feedback and mergers push this gas efficiently beyond the virial radius. Around  $z = 1.5$ , the inflow-to-outflow channel is overtaken by a different pathway: gas particles undergo gradual heating during and after crossing the virial radius. This is also the time when the halo of Eris exceeds the critical mass necessary to develop a stable shock at  $0.1 R_{\text{vir}}$ . Outside the virial radius, it is common that the temperature of gas particles sharply increases with no shift in the radial location. These particles also receive no SNe energy, suggesting shock-heating as the relevant heating agent.

In what follows, we quantify the difference that the presence of SN feedback makes on the diffuse gas budget and its evolution. In order to achieve that, we perform a direct test of the impact of SN feedback on the halo; namely, we run another simulation, which is a variation of Eris but without SN feedback (hereafter this run is referred to as ErisNFB). We chose  $z = 4$  to be the

starting redshift to compromise between the two requirements: 1) the diffuse gaseous halo should ideally be absent; 2) lack of feedback should have as little influence on the assembly history as possible. Although without feedback one cannot produce realistic galaxies due to overcooling, the benefit of this test lies in being able to isolate the effect of SN heating from gravitational heating by accretion shocks and merger-induced shocks.

Figure 11 illustrates a violent heating episode, which is an example of a series of such events occurring repeatedly over the lifetime of a galaxy, and compares its magnitude between a run with feedback (top row) and without (bottom row). The temperature maps in Figure 11 capture the evolution of the “blast” over 0.3 Gyr in the environment of Eris; however, similar occurrences are also common in Venus. In both Eris and ErisNFB, the general sequence is similar: at  $z = 3.42$ , the gaseous halo consists of two blobs of warm-hot gas that are separated by inflows of cold/warm gas. The central concentration of over one million-degree gas grows significantly into a nearly spherical region, attaining an extent of approximately 20 kpc by  $z = 3.26$ . Afterwards, the inner part of the halo expands and cools. Early “blasts” in Eris are easy to detect in the temperature maps, and their timing is coincidental with the peaks in the star formation rate (see Figure B1 in the Appendix).

The second row of Figure 11 shows that hot gas can also be generated much earlier than what is expected based on conventional cold/hot mode threshold even in the absence of feedback. Already at  $z = 3.42$ , gas in the center of ErisNFB exceeds the temperature threshold of  $10^6$  K. Here, powerful outflows are generated during a major merger, seen in the map as conical warm-hot and hot patches, which reach distances exceeding the virial radius of a galaxy. The metal-poor outflows generated without feedback are triggered by shock-heating associated with mergers. However, those outflows are much less powerful than those combined with SN feedback, as they have a limited range compared with the heat maps

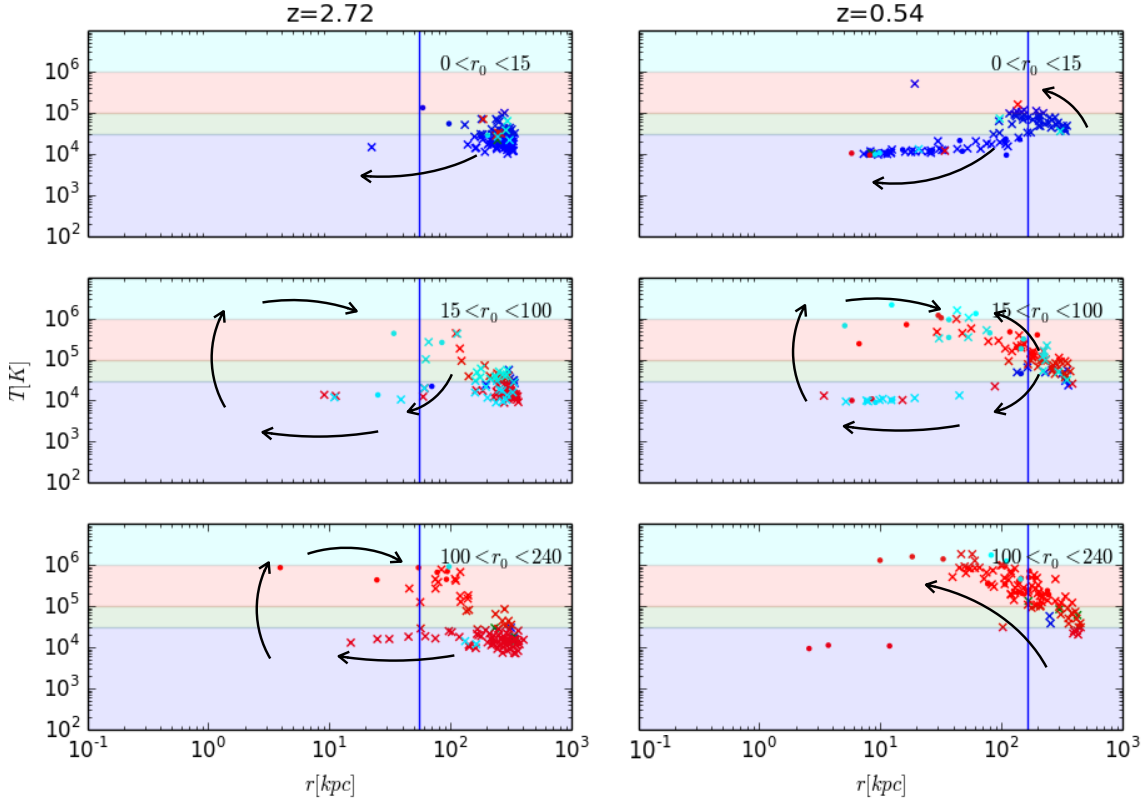


**Figure 10.** Radius-temperature diagram for a selection of particles from  $z = 0$  traced back in time to  $z = 2.72$  (left column) and  $z = 0.54$  (right column). Each row distinguishes between particles which build a different region of a gaseous halo at  $z = 0$  (top to bottom:  $r_0 < 15$  pkpc,  $r_0 \in (15, 100)$  pkpc,  $r_0 \in (100, 240)$  kpc). Background of each panel is color-coded according to the temperature range of each phase of gas (hot, warm-hot, warm, cold) and particle color-coding represents their end state at  $z = 0$ . Arrows mark the typical trajectories of particles in these two accretion epochs. Individual particles are marked with a dot or a cross, depending on whether they receive feedback energy or not (dot = yes). Vertical line marks the virial radius. For a detailed description of the experiment, including the selection method, see the text. Case study: Eris.

of Eris at  $z = 2.99$ . This result indicates that SN feedback has a significant impact on the gas distribution of a gaseous halo even as early as  $z = 3.5$ .

In Figure 12, we show the radial density profiles of the two gas phases: warm-hot (top) and hot (bottom) for the run with SN feedback (solid lines) and without (dashed lines) at  $z = 3$  and  $z = 2$ . The presence of feedback makes a major difference in the center of a diffuse halo ( $\sim 0.1R_{\text{vir}}$ ), in particular in the warm-hot phase. The density of the warm-hot gas in that region is about 2 orders of magnitude higher if SN feedback is switched on. The discrepancy between the density of hot gas in Eris and ErisNFB is smaller but also significant, namely hot gas is about 5 times denser in Eris than in ErisNFB. Beyond  $\sim 0.1R_{\text{vir}}$ , density profiles of both gas phases tend to converge (warm-hot at  $\sim R_{\text{vir}}$  and hot at  $\sim 0.4R_{\text{vir}}$ ). Overall, a run with supernovae feedback switched on produces more hot gas. For exam-

ple, already at  $z = 3$  we find 1.3 times more hot gas in Eris than in ErisNFB within the virial radius, and by  $z = 1$  that ratio increases to 1.5. In total, introducing feedback increased the abundance of  $T > 10^5$  K gas by a factor of 1.3-1.4 between  $z = 3 - 1$  within the virial radius.

Halos are not only structurally different but also imply a different X-ray evolution with redshift. We compute X-ray luminosities at  $z = 3, 2, 1$  in the 0.5-2 keV band for Eris and ErisNFB using the same procedures as described in the beginning of the section 3. We find that X-ray luminosities are higher when feedback is included, namely  $3.40 \times 10^{41}$ ,  $8.9 \times 10^{40}$ ,  $5.9 \times 10^{40}$  erg/s as opposed to  $2.4 \times 10^{38}$ ,  $1.1 \times 10^{38}$ ,  $1.3 \times 10^{37}$  erg/s at  $z = 3, 2, 1$  respectively. Lack of feedback thus likely violates the X-ray luminosity constraints on the present-day halos, suggesting that SN feedback is not only essential to obtain realistic disk galaxies but also their diffuse halos.

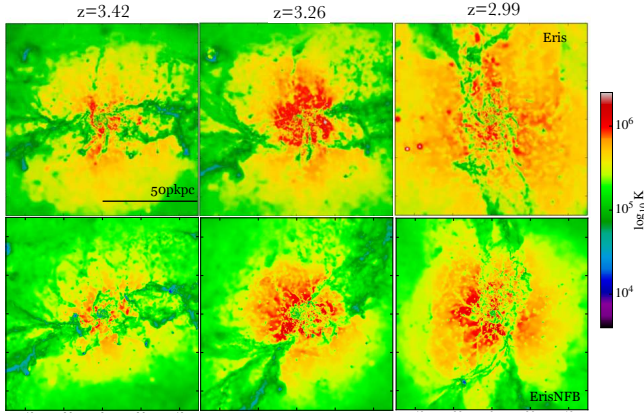


**Figure 11.** Temperature maps of a gaseous halo at 3 timesteps, illustrating a typical “blast” in action in case with feedback (Eris) and without (ErisNFB). Red regions (hot gas, first and second subplots) cool down and expand adiabatically over time (orange-yellow regions in the last subplot). The width of each square is 100 pkpc.

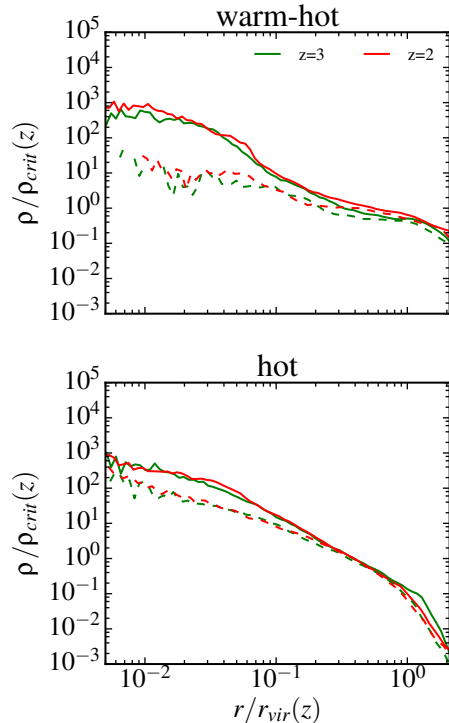


**Figure 12.** Density profiles of warm-hot (top) and hot (bottom) with SN feedback (solid lines) and without (dashed lines). The normalization of the axes are critical density of the universe and virial radii of halos at the corresponding redshifts.

### 3.3. Coronae and cold flows

As discussed in the introduction, Milky Way-like galaxies occupy a mass scale, at which galaxies are expected to acquire gas initially via the “cold mode” and then, via the “hot mode”. Two effects are at play in building up the diffuse halo and driving the transition from cold filamentary accretion to hot spherical accretion: 1) halos grow sufficiently in mass beyond a threshold, after which a stable shock develops, thereafter heated accretion occurs; 2) initially compact filaments thicken over time; as they reach a cross section that is comparable with that of the halos, they lose the ability to penetrate gaseous halos down to a galaxy. This work adds a new factor to this framework, namely it emphasizes the importance of the processes heating the gas inside-out. Energy injections from mergers and supernovae explosions lead to an earlier formation of the diffuse halos than what was previously established, and in halos of mass much lower than the critical mass of  $\sim 10^{12} M_{\odot}$ .

The remaining question is whether the presence of those early diffuse halos affects the galaxy-filaments connection and thus the accretion mode switch, which we touch upon in this section.

Early on, hot and warm-hot gas phases are outflowing, which is a consequence of their origin. An early gaseous halo thus can be thought of as hosting two fronts on a collisional trajectory: cold dense filamentary flows with a negative radial velocity, and an expanding diffuse halo with a positive radial velocity. Naturally, those two fronts will exchange momentum and energy upon a collision. In Figure 13, we show that the inside-out growing corona shields a galaxy from the cold flows. Following the literature, we define the *cold flow* to be the gas at temperatures below  $10^5$  K that is moving towards the galactic center; gas at  $T > 10^5$  K is assigned to the diffuse halo. Ram pressure,  $p_{ram}$ , is defined as  $p_{ram} = \frac{1}{2} \rho v_r^2$ , and thermal pressure,  $p_{th}$ , is given by  $p_{th} = \frac{kT\rho}{\mu m_p}$ . Figure 13 illustrates how the ratio of the total pressure (sum of thermal and ram pressure) of the diffuse halo and the cold flows ( $p_{wh}/p_{cf}$ ) is reversed in the immediate vicinity of the galaxy over time.

Initially, cold flows penetrate the galactic halo and easily reach the disk. The filamentary structure of Eris at  $z = 3$  consists of branches, which clearly mark preferential directions of accretion, whereas Venus is bombarded by such flows from nearly all directions, although after a few Gyrs, Venus exhibits the same pattern as Eris. Namely, the energy released from the center of the halo gradually generates a thermally pressurized central bubble, which expands outward and engulfs the filaments. A cold filament in Eris at  $z = 2$  behaves analogically to the river mouth that widens upon encountering

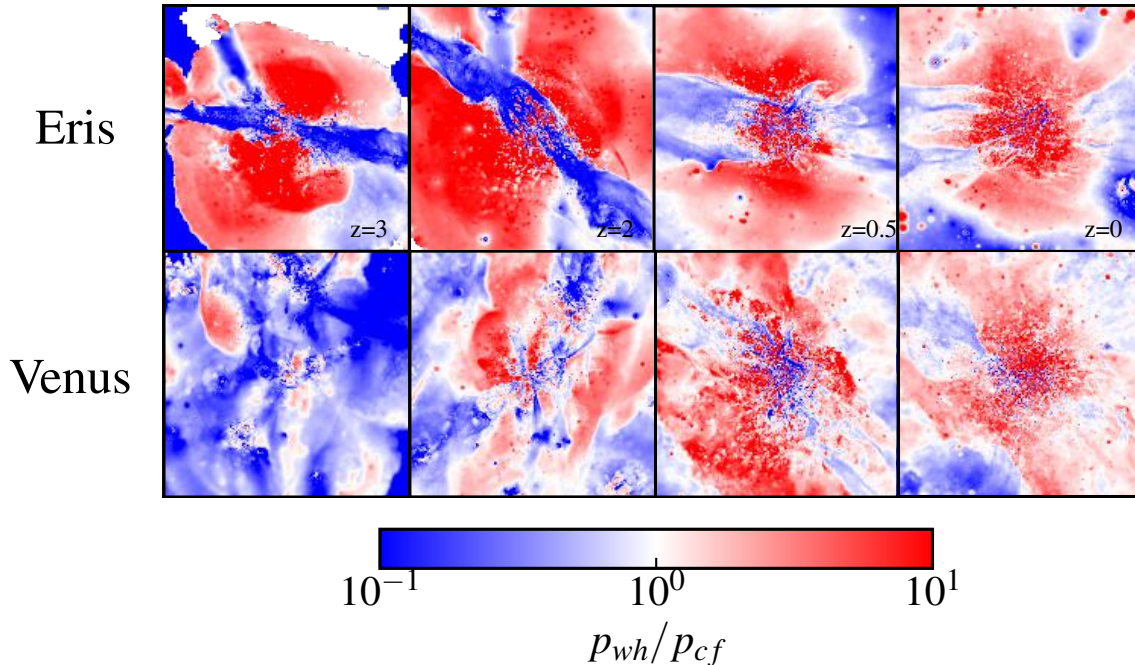


**Figure 13.** Evolutionary sequences of the total pressure fractions of the "warm-hot accretion" (a sum of ram and thermal pressure) to the total pressure of the "cold flow". A width of each square is 1 pMpc.

an obstacle (hot corona), and tries to flow through it and around it via paths of least resistance. These accretion channels become thinner over time (examples of such narrow streams are shown at  $z = 0.5$ ,  $z = 0$  in Figure 13). Note the nearly spherically symmetric distribution of the ratio  $p_{wh}/p_{cf}$  after  $z = 2$ , when the outflow-induced corona driven by both mergers and feedback outbalances the pressure of the filaments. Additionally, filaments are weakened in structure by the ram pressure stripping that acts with a magnitude of velocity that is a sum of both fronts (e.g. before  $z = 2$ ,  $|\frac{v_{wh}}{v_{cf}}| \lesssim 10$ ).

We showed in section 3.2 that inclusion of SN feedback increases the density of diffuse gas near the galaxy by up to two orders of magnitude. Hereafter, we describe qualitatively the consequences of efficient SN feedback for the galaxy-cold flow connection. Figure 14 presents the temperature maps of gas in a face-on view on the central galaxy. The width of each square is 500 comoving Mpc. Top row shows a few early snapshots of the Eris simulation and is set against the snapshots of ErisNFB in the bottom row in order to show the structural differences in the halo at the absence of feedback.

Looking first at Eris results (top row), focused streams of intergalactic material initially easily reach and feed the galactic disk of Eris (a, top row of Fig. 14). Prominent outflows isolate the central galaxy from the filamentary network for extended periods of time (b, the pushback region is marked by two dashed lines). After some time, filaments continue loading cold gas, however,

via scattered channels (c). Their structure is also notably weakened already at  $z = 2.99$ . The growth of hot coronal gas (i.e. of the thermal and ram pressure front) gradually pushes filaments back and away from a galaxy (d,e). Compared with Eris, the diffuse gas of ErisNFB develops a visibly weaker pressure front (bottom row of Fig. 14). Feedback-supported pressure front forces filaments, even if temporarily, to much larger distances (columns b, d, e; compare top and bottom of Fig. 14). Feedback also heats up and strips filaments already as early as  $z = 3.83$  (columns a,c circles). Thus, SN feedback not only charges coronae with additional hot material but also affects the intersection corona-filament in a way that efficiently isolates a galaxy from the cold inflow. We expect this mechanism to regulate star formation and make it less efficient (either temporarily or permanently). The exact details of this mechanism, however, will be studied in the future work.

#### 4. CONCLUSIONS

In this paper, we use a set of 3 hydrodynamical zoom-in simulations of Milky Way-sized halos ( $M_{halo} \lesssim 10^{12} M_{\odot}$ ) in order to investigate the formation of X-ray luminous gas around these galaxies. Two of our runs are variations of the default Eris simulation: 1) the SN feedback mechanisms are switched off, which allows for quantifying the effect of SN feedback on the halo evolution (ErisNFB); 2) the initial conditions are changed, providing a case study of active merger history (Venus).

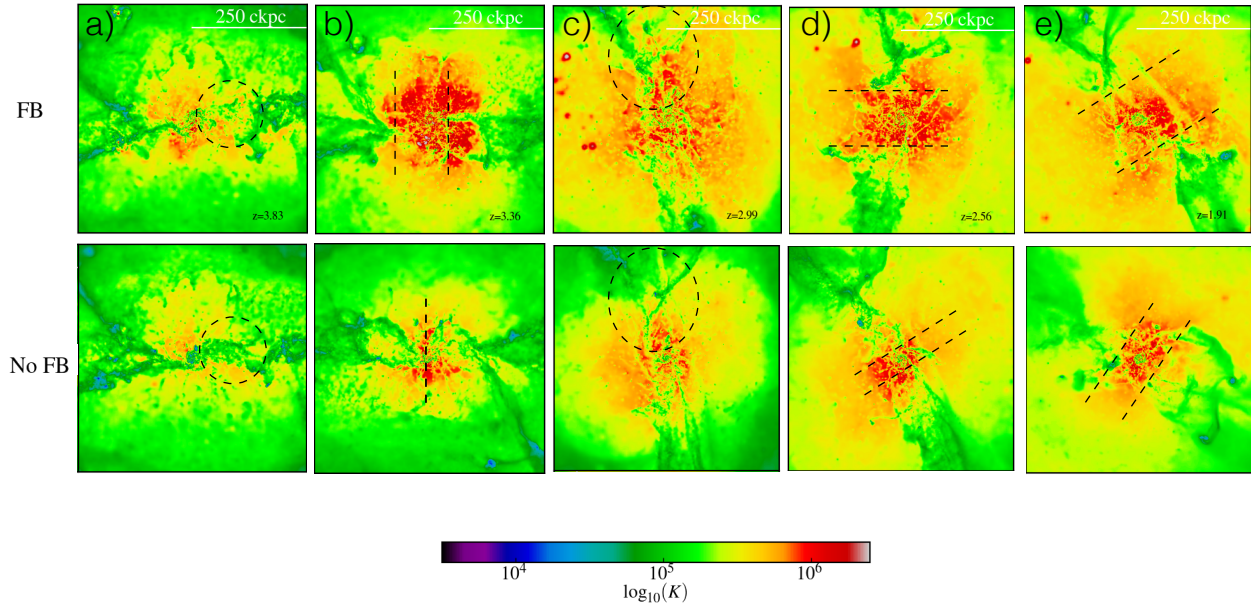


**Figure 14.** Temperature maps of Eris (top row) and ErisNFB (bottom row) between  $z \sim 4$  and  $z \sim 2$  comparing the change in the location (lines, columns b, d and e) and structure (circles, columns a and c) of the filaments with and without feedback.

In Paper I of this series, we studied present-day diffuse halos of simulated galaxies and matched them against available constraints on the Milky Way. This paper (Paper II) investigates how these diffuse halos form. In particular, we focus on two gas phases: hot ( $T > 10^6$  K) and warm-hot ( $T = 10^{5-6}$  K) that have different characteristics. For example, we showed in Paper I that hot coronae are localized within  $0.4 R_{vir}$  of their halos, while the warm-hot gas stretches to beyond  $2-3R_{vir}$ . We explain this configuration in physical terms.

1. We investigated when halos of our realistic galaxies (Eris, Venus) enter the critical mass regime for the development of the stable shock at  $0.1$  and  $1.0 R_{vir}$ . We compared the resulting redshift with the time, during which hot diffuse atmospheres of gas begin to appear around those halos. We found that diffuse halos can develop earlier than is expected in the standard picture (White & Frenk 1991; Dekel & Birnboim 2006), even as early as  $z = 4 - 3$ , but also in low-mass halos. The most striking example is Venus, as its halo mass, for instance at  $z = 3$ , is about an order of magnitude below the critical mass threshold of few times  $10^{11} M_{\odot}$ . This opens a question of how galaxies build hot reservoirs of gas via alternative channels. Two other heating mechanisms we put forward are merger-induced shocks and SN heating.

2. Hot coronae are built by gas crossing  $R_{vir}$  across all redshifts. Most of this accretion is cold at high redshifts when it passes the virial radius the first time. This cold-accreted gas must then be heated to over a million degrees in order to become a part of the hot corona. The halo mass is too small to sustain a stable shock at  $0.1R_{vir}$ , therefore we conclude that cold-accreted gas must be shock-heated via mergers and the energy of supernovae. It could then remain in the diffuse state with a long cooling time, or be ejected outside the virial radius and return as the second-generation hot accretion at later times.

3. The onion-like structure (a hot corona embedded in a warm-hot envelope of gas) develops after  $z = 2$ . The warm-hot envelope forms at the intersection of two fronts: 1) the expanding and adiabatically cooling hot gas; 2) the IGM accretion of warm-hot gas, which becomes possible as soon as a halo mass crosses the critical mass for the development of a stable shock. Since hot gas is converted into the warm-hot phase during the adiabatic expansion, the density profile of hot gas begins to drop off sharply. Simultaneously, the density of warm-hot gas develops an inflection point around  $0.2 - 0.3R_{vir}$  and a local maximum (a conglomerate of the two fronts). The size of an adiabatically cooling hot corona decreases with time to  $0.4R_{vir}$

at  $z = 0$ .

4. A direct measurement of energy injection rates reveals that the heating of the warm-hot gas is dominated by supernovae across all redshifts, while the second-most important heating source is artificial viscosity (lower within a factor of two). The energy rates for hot gas show that SN are at least as important as other heating mechanisms generating shocks (artificial viscosity). Hot gas is also most metal-enriched at all evolutionary stages ( $z = 7, 3, 0.5$ ).

In order to determine whether coronae can form in the absence of feedback, we ran a high-resolution cosmological simulation without SNe feedback (ErisNFB) from  $z = 4$ . Switching off feedback allows for isolating SN heating from gravitational heating by accretion shocks and merger-induced shocks. Below are our major findings.

1. The metal-poor hot outflows can be generated without feedback, and they are likely triggered by mergers. However, outflows are much more powerful and have a greater range when SN feedback is present, even as early as  $z = 3.5$ . This is why diffuse halos can form earlier and in considerably lower mass halos than expected. Feedback and no-feedback runs should align as halos reach a critical mass for the development of a stable shock.
2. Already at  $z = 3$  we find 1.3 times more hot gas within the virial radius in the simulation with feedback compared to the same run without feedback, and by  $z = 1$  that ratio increases to 1.5. Introducing feedback also increased the abundance of  $T > 10^5$  K gas by a factor of 1.3-1.4 between  $z = 3 - 1$  and within the virial radius. The presence of feedback makes a major difference in the center of a diffuse halo (within  $\sim 0.1R_{\text{vir}}$ ); the density of the warm-hot gas in that region is about 2 orders of magnitude higher if SN feedback is switched on. Hot gas in the center of Eris is about 5 times denser than in ErisNFB.
3. The X-ray luminosity of our gaseous halos without SN feedback is lower than with feedback by two orders of magnitude. Eris with SN feedback attains  $3.40 \times 10^{41}$ ,  $8.9 \times 10^{40}$ ,  $5.9 \times 10^{40}$  erg/s at  $z = 3, 2, 1$  respectively. Our results imply that low-luminosity spirals with  $M_*$  and  $M_{\text{halo}}$  similar to the progenitors of Eris and Venus at  $z > 2$ , and with similar star formation rates, should be surrounded by the extended X-ray emitting gas.

In this work we also emphasized on the connection between coronae and the accretion bimodality of Milky

Way-like galaxies. We investigate what happens at the intersection of growing hot gas concentrations and cold filaments, and the role of feedback therein. Our findings are summarized in the points below.

1. The growth of a corona cuts a galaxy off the filamentary network. It happens due to change in the pressure balance around the galaxy – an outflow-induced corona (from both mergers and feedback) outbalances the pressure of the filaments. The pressure bubble propelled by galactic outflows pushes the filaments (cold flows) away, and at the same time ram pressure strips the filaments with the relative velocity of the expanding bubble and the inflow. Thus, the growth of a corona might be responsible for the accretion mode switch. The switch happens gradually – a galaxy accretes cold IGM material via narrow channels, these channels are however weakened and progressively stripped as they pass through a high-pressure medium.
2. We showed that SN feedback not only charges coronae with additional hot material but also affects the intersection corona-filament in a way that efficiently isolates a galaxy from the cold inflow. This has also consequences for the large-scale gas supply, and may contribute to quenching of galaxies.

The most important finding of this work is that *a galactic corona is not a consequence of hot spherical accretion onto a galaxy*. The corona is a consequence of mergers-induced shock heating and feedback, grows inside-out, is X-ray luminous and detaches a galaxy from the filamentary network.

All this is quite different from the mainstream picture, in which hot mode accretion is a consequence of thermalisation of kinetic energy derived from gravity. It is possible that at larger mass scales, gravitational compression and stable shocks play a more important role than supernovae feedback or mergers. However, the picture drawn in this paper is more relevant for typical spiral galaxies with the virial mass near  $10^{12}M_{\odot}$ . Future X-ray surveys sensitive to such mass scale will test this model.

This study leaves a few open questions. For example, it is still unclear how the hot IGM accretion is affected by the presence of SN feedback at the virial and galactic radii. As we are expecting outflows to leave the halo at early redshifts, it is possible that the recurrent accretion (circulation flows) is additionally contributing to the hot accretion as early as  $z = 3 - 4$ . The recurrent accretion could be metal-enriched by feedback or also metal-poor, if it originates in major mergers. Perhaps both factors

would alter the time of the accretion mode switch. These topics have yet to be investigated in the future work.

## 5. ACKNOWLEDGEMENTS

Authors would like to thank Simon White, Andrey Kravtsov, Cristal Martin, Jerry Ostriker, Joop Schaye, Ali Rahmati, Sebastian Trujillo-Gomez, Mike Fall, Neal Katz and Carlos Frenk for their insights that helped complete this study. L.M. thanks the Kavli Institute for

Theoretical Physics at UC Santa Barbara for hospitality during the ‘‘Galaxy-Halo Connection’’ Program in Spring 2017, during which preliminary results of this work were presented and thoroughly discussed. AB acknowledges support from NSERC (Canada) through the Discovery Grant program and from the Pauli Center for Theoretical Studies ETH UZH, and is grateful to the University of Zurich’s Institute for Computational Sciences, and especially the members of the Institute’s Center for Theoretical Astrophysics and Cosmology, for their hospitality during his recent extended visit.

## APPENDIX

In this Appendix, we discuss what happens in the models, in which SN feedback is excessively boosted to quench star formation at early times. First, we describe the parameters of an additional simulation, a variation of Eris with strong supernovae feedback. Then, we discuss its outcome in the context of several observables and main results of this paper.

### A. SIMULATION WITH STRONG FEEDBACK: DESCRIPTION

Eris2k (hereafter E2k, described in more detail in [Sokolowska et al. 2016](#)), stems from the same initial conditions as Eris but differs in the choice of some sub-grid parameters. Its parameters were tuned in order to yield a stronger effect of supernova (SN) feedback to lower star formation rates at high redshift. E2k also has a richer inventory of physical processes, including not only metal-line cooling but also a sub-grid turbulent diffusion prescription for both metals and thermal energy which allows mixing to be captured in SPH ([Shen et al. 2010](#)). Some of the important simulation parameters of E2k and other runs of this paper, including the choice of the UV background and aspects of the sub-grid physics, are listed in [Table A1](#) and discussed below.

In contrast to Eris and Venus, the metal-line cooling in E2k is computed at all temperatures, employing tabulated rates computed with the code CLOUDY ([Ferland et al. 1998](#)), under the assumption that metals are in ionization equilibrium ([Shen et al. 2010](#)). We also use the updated cosmic ionizing background ([Haardt & Madau 2012](#)). The recipes for star formation and SN feedback are the same in all the runs and are described in [Stinson et al. \(2006\)](#) but there are a few differences in associated parameters. Namely, the star formation threshold  $n_{\text{SF}}$  of E2k is set to  $100 \text{ cm}^{-3}$ ; the maximum temperature of a particle allowed for star formation is  $T_{\text{max}} = 3 \times 10^4 \text{ K}$ ; supernova efficiency parameter is increased to  $\epsilon_{\text{SN}} = 1.0$ ; and the initial mass function is updated to ([Kroupa 2001](#)) (see [Table A1](#)).

The strength of feedback depends on the number of SNe produced, which is in turn governed by the IMF and, locally, by the star formation density threshold. An updated IMF yields about a factor of 2.8 more SNe at equivalent star formation rate than Eris/Venus. Furthermore, as explained in detail in [Guedes et al. \(2011\)](#) and [Mayer \(2012\)](#), the local star formation rate, and thus the local effect of SNe, can be boosted significantly by raising the star formation density threshold as the interstellar medium is allowed to become more inhomogeneous, an effect that saturates only at very high resolution and density thresholds, well above those resolved in cosmological simulations ([Hopkins et al. 2012](#)). This implies that in E2k, heating by SN feedback is boosted both globally and locally. We recall that E2k is a run that follows an extensive study of sub-grid parameters by running many different simulations with the same Eris-type initial conditions in order to determine the combination of parameters that yields realistic stellar masses in accordance with abundance matching at both high and low redshift, these being shown in [Table A1](#).

Run	UVB	IMF	$n_{\text{SF}}$	$\epsilon_{\text{SN}}$	MC	IC
Eris	HM96	K93	5	0.8	low-T	Q
E2k	HM12	K01	100	1.0	all-T	Q
Venus	HM96	K93	5	0.8	low-T	A

**Table A1.** Input parameters of the runs. Notation: UVB – UV background (HM96: [Haardt & Madau 1996](#), HM12: [Haardt & Madau 2012](#)), IMF – initial mass function (K93: [Kroupa et al. 1993](#), K01: [Kroupa 2001](#)),  $n_{\text{SF}}$  – star formation density threshold in  $\text{cm}^{-3}$ ,  $\epsilon_{\text{SN}}$  – SN efficiency parameter in  $10^{51} \text{ erg}$ , MC – metal cooling, and IC – initial conditions (Q: quiet merger history, A: active merger history).



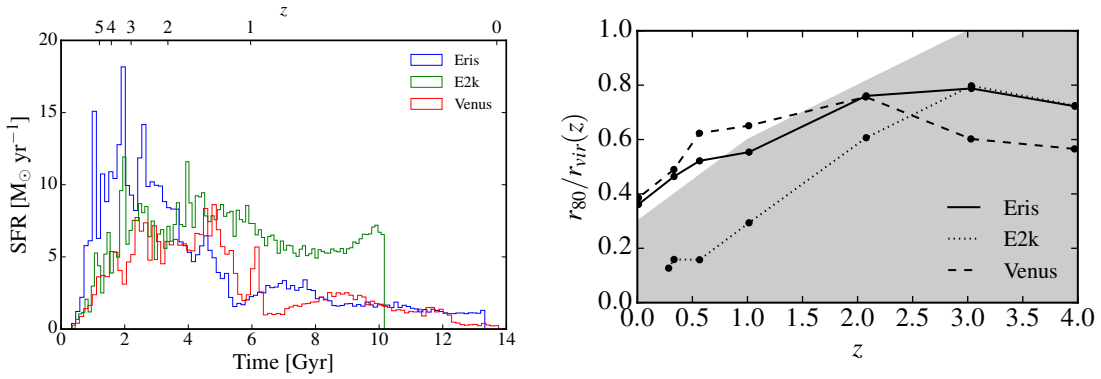


**Figure B1.** Left. The comparison of star formation histories of Eris, E2k and Venus. Note that the run E2k was stopped after 10 Gyrs of evolution. Right. The radius of a hot corona encompassing 80% of its mass as a function of redshift.

## B. IMPACT OF STRONG FEEDBACK ON OUR MAIN RESULTS

*Star formation history.* — In the left panel of Figure B1, we compare star formation histories of Eris, Venus and E2k. Eris and Venus differ at early times (Eris has much higher star formation rate until  $z = 2$ ; the star formation of Venus is delayed with respect to Eris because of its late assembly history). The assembly history of E2k is the same as Eris, however, the differences lie in the subgrid physics, which is discussed above. Feedback was boosted in E2k in order to quench star formation at early times, and hence be closer to the abundance matching. This works well until approximately 8 Gyrs, after which the model breaks down. The material, which was ejected via strong winds, turns around and feeds the star formation, which begins to increase to several times the star formation rate of the Milky Way.

*Radius of the corona  $r_{80}$ .* — In the right panel of Figure B1, we compare the radius encompassing 80% of a hot corona between Eris, Venus and E2k. After  $z = 3$ ,  $r_{80}$  of E2k begins to shrink to less than a half of the size of the remainder. At the same time, we showed in Paper I that the present-day hot mass budget of both E2k amounts to 1%  $M_{\text{vir}}$ , similarly to other runs in this study. This means that a corona of E2k is much more compact.

*X-ray luminosity.* — The X-ray luminosity of diffuse gas in the 0.5-2 keV band is a mismatch with the known constraints on the Milky Way discussed in this paper, namely it is about 100 times higher than that ( $L_X \sim 10^{42} \text{ erg/s}$ ). In Paper I, we linked this result with a too-strong feedback.

*Summary.* — Early ejective feedback quenches star formation until late epochs, when the gas turns around and begins to feed star formation at a high level. This affects not only the observables for the galactic disk, but also the diffuse gaseous halo, which turns out to be too metal-enriched, and produces too many X-rays due to the compactness of its hot halo.

## REFERENCES

- Agertz, O., & Kravtsov, A. V. 2015, *ApJ*, 804, 18  
 Anders, E., & Grevesse, N. 1989, *GeoCoA*, 53, 197  
 Anderson, M. E., & Bregman, J. N. 2011, *ApJ*, 737, 22  
 Bertschinger, E. 2001, *ApJS*, 137, 1  
 Binney, J. 1977, *ApJ*, 215, 483  
 Birnboim, Y., & Dekel, A. 2003, *MNRAS*, 345, 349  
 Bogdán, Á., Forman, W. R., Kraft, R. P., & Jones, C. 2013, *ApJ*, 772, 98  
 Bogdan, A., Forman, W. R., Vogelsberger, M., et al. 2013, *ApJ*, 772, 97  
 Bower, R. G., Benson, A. J., & Crain, R. A. 2012, *MNRAS*, 422, 2816  
 Bregman, J. N., & Lloyd-Davies, E. J. 2007, *ApJ*, 669, 990  
 Bromm, V., Ferrara, A., Coppi, P., & Larson, R. B. 2001, *MNRAS*, 328, 958  
 Brooks, A. M., Governato, F., Quinn, T., Brook, C. B., & Wadsley, J. 2009, *ApJ*, 694, 396  
 Dekel, A., & Birnboim, Y. 2006, *MNRAS*, 368, 2  
 Dekel, A., Birnboim, Y., Engel, G., et al. 2009, *Nature*, 457, 451  
 Fang, T., Buote, D. A., Bullock, J. S., & Ma, R. 2015, *ApJS*, 217, 21  
 Fardal, M. A., Katz, N., Gardner, J. P., et al. 2001, *ApJ*, 562, 605  
 Ferland, G. J., Korista, K., Verner, D., et al. 1998, *PASP*, 110, 761  
 Fiacconi, D., Feldmann, R., & Mayer, L. 2014, *MNRAS*, 446, 1957  
 Guedes, J., Callegari, S., Madau, P., & Mayer, L. 2011, *ApJ*, 742, 76  
 Gupta, A., Galeazzi, M., Koutroumpa, D., Smith, R., & Lalleme, R. 2009, *ApJ*, 707, 644  
 Haardt, F., & Madau, P. 1996, *ApJ*, 461, 20  
 —. 2012, *ApJ*, 746, 125  
 Hahn, O., & Abel, T. 2011, *MNRAS*, 415, 2101  
 Henley, D. B., & Shelton, R. L. 2013, *ApJ*, 773, 92

- Hopkins, P. F., Quataert, E., & Murray, N. 2012, *MNRAS*, 421, 3488
- Kaastra, J., Finoguenov, A., Nicastro, F., et al. 2013, *ArXiv e-prints*, arXiv:1306.2324
- Katz, N., Keres, D., Dave, R., & Weinberg, D. H. 2003, in *Astrophysics and Space Science Library*, Vol. 281, *The IGM/Galaxy Connection. The Distribution of Baryons at  $z=0$* , ed. J. L. Rosenberg & M. E. Putman, 185
- Kereš, D., Katz, N., Fardal, M., Davé, R., & Weinberg, D. H. 2009, *MNRAS*, 395, 160
- Kereš, D., Katz, N., Weinberg, D. H., & Davé, R. 2005, *MNRAS*, 363, 2
- Kroupa, P. 2001, *MNRAS*, 322, 231
- Kroupa, P., Tout, C. A., & Gilmore, G. 1993, *MNRAS*, 262, 545
- Marinacci, F., Pakmor, R., & Springel, V. 2014, *MNRAS*, 437, 1750
- Mashchenko, S., Wadsley, J., & Couchman, H. M. P. 2007, *Science*, 319, 174
- Mayer, L. 2012, in *Advances in Computational Astrophysics: Methods, Tools, and Outcome*, ed. R. Capuzzo-Dolcetta, M. Limongi, & A. Tornambè, Vol. 453 (*Astronomical Society of the Pacific Conference Series*), 289
- McKee, C. F., & Ostriker, J. P. 1977, *ApJ*, 218, 148
- Miller, M., & Bregman, J. 2013, *ApJ*, 770, 13
- Miller, M. J., & Bregman, J. N. 2014, *ApJ*, 800, 14
- Peeples, M. S., Werk, J. K., Tumlinson, J., et al. 2014, *ApJ*, 786, 54
- Puchwein, E., & Springel, V. 2013, *MNRAS*, 428, 2966
- Putman, M. E., Peek, J. E. G., & Jounge, M. R. 2012, *ARA&A*, 50, 491
- Putman, M. E., Staveley-Smith, L., Freeman, K. C., Gibson, B. K., & Barnes, D. G. 2003, *ApJ*, 586, 170
- Rasmussen, J., Sommer-Larsen, J., Pedersen, K., et al. 2009, *ApJ*, 697, 79
- Rees, M. J., & Ostriker, J. P. 1977, *MNRAS*, 179, 541
- Roškar, R., Teyssier, R., Agertz, O., Wetzstein, M., & Moore, B. 2014, *MNRAS*, 444, 2837
- Sedov, L. I. 1959, *Similarity and Dimensional Methods in Mechanics*
- Sembach, K. R. 2006, in *The Local Group as an Astrophysical Laboratory*, ed. M. Livio & T. M. Brown, Vol. 17, 86 – 99
- Shen, S., Madau, P., Aguirre, A., et al. 2012, *ApJ*, 760, 50
- Shen, S., Madau, P., Conroy, C., Governato, F., & Mayer, L. 2014, *ApJ*, 792, 99
- Shen, S., Wadsley, J., & Stinson, G. 2010, *MNRAS*, 407, 1581
- Smith, R. K., Brickhouse, N. S., Liedahl, D. A., & Raymond, J. C. 2001, *ApJL*, 556, L91
- Snowden, S. L., Egger, R., Freyberg, M. J., et al. 1997, *ApJ*, 485, 125
- Sokołowska, A., Capelo, P. R., Fall, S. M., et al. 2017, *ApJ*, 835, 289
- Sokołowska, A., Mayer, L., Babul, A., Madau, P., & Shen, S. 2016, *ApJ*, 819, 21
- Somerville, R. S., & Davé, R. 2015, *ARA&A*, 53, 51
- Stinson, G., Seth, A., Katz, N., et al. 2006, *MNRAS*, 373, 1074
- Taylor, G. 1950, *Proceedings of the Royal Society of London Series A*, 201, 159
- Tumlinson, J., Thom, C., Werk, J. K., et al. 2011, *Science*, 334, 948
- van de Voort, F., Quataert, E., Hopkins, P. F., et al. 2016, *MNRAS*, 463, 4533
- Wadsley, J., Stadel, J., & Quinn, T. 2004, *New Astron.*, 9, 137
- Wang, Q. D. 1998, in *Lecture Notes in Physics*, Berlin Springer Verlag, Vol. 506, *IAU Colloq. 166: The Local Bubble and Beyond*, ed. D. Breitschwerdt, M. J. Freyberg, & J. Truemper, 503–512
- Wang, Q. D., Yao, Y., Tripp, T. M., et al. 2005, *ApJ*, 635, 386
- White, S. D. M., & Frenk, C. S. 1991, *ApJ*, 379, 52
- White, S. D. M., & Rees, M. J. 1978, *MNRAS*, 183, 341